Comparative analysis between CFD model and DHLLDV model in fully-suspended slurry flow

Ting, Xiong; Miedema, Sape A.; Xiuhan, Chen

DOI
10.1016/j.oceaneng.2019.03.065

Publication date
2019

Document Version
Final published version

Published in
Ocean Engineering

Citation (APA)
Ting, X., Miedema, S. A., & Xiuhan, C. (2019). Comparative analysis between CFD model and DHLLDV model in fully-suspended slurry flow. *Ocean Engineering*, *181*, 29-42. https://doi.org/10.1016/j.oceaneng.2019.03.065

Ocean Engineering 181 (2019) 29–42

Contents lists available at ScienceDirect

Ocean Engineering

journal homepage: www.elsevier.com/locate/oceaneng

Comparative analysis between CFD model and DHLLDV model in fully-suspended slurry flow

Xiong Ting[a,b], Sape A. Miedema[b], Chen Xiuhan[b,*]

[a] School of Energy and Power Engineering, Wuhan University of Technology, Wuhan, Hubei, 430063, PR China
[b] Section Offshore and Dredging Engineering, Delft University of Technology, Mekelweg 2, Delft, Netherlands

ARTICLE INFO

Keywords:
Fully-suspended slurry flow
Concentration distribution
Hydraulic gradient
DHLLDV
CFD

ABSTRACT

The behavior of fully-suspended slurry flow in horizontal pipeline can be simulated through two very distinct models, the Computational Fluid Dynamics (CFD) model and the Delft Head Loss & Limit Deposit Velocity (DHLLDV) model. The predicted results from simulations are compared with a series of experiment data from the literature, involving the effects of different particles volume concentration (9–42%), particle size (90–440 μm), mixture velocity (1–9 m/s), and pipe diameter (51.5–263 mm) on hydraulic gradient and particles concentration distribution, and revealing excellent agreements between two model predictions and the experimental data. Both CFD and DHLLDV, however, still have some deviations in the near-wall concentration distribution as for larger particles. Though it is observed that the accuracy for CFD will decline when particle size increases and further research is needed for improving the accuracy of the models for the near-wall flow of larger particles, it can be concluded that both CFD model and DHLLDV model apply to calculations for fully-suspended flow.

1. Introduction

Slurry pipeline transport has gained its wide application in many engineering fields like dredging, mining and chemistry due to its efficiency and economy. It is worthwhile to do research on rheological properties, particle dynamics and resistance characteristics to reduce pipeline resistance, avoid pipe blockage and increase the transport distance. It is also what the recent researchers are working on and therefore many simplified empirical formulas have been put forward. But limitations appear because these formulas are different and have to be applied respectively to their own slurry and transport conditions. Obviously, it is urgent to find a unified and convenient model applying to different slurries and different transport conditions which are quite common in real dredging. The Delft Head Loss & Limit Deposit Velocity (DHLLDV) model put forward by Miedema (2016), was established by summarizing and modifying many previous models. The DHLLDV model can not only identify different flow regimes according to the range of flow speed, but also make corresponding calculations for different flow regimes. At the same time, with the rapid-developing computer technology, another method, the Computational Fluid Dynamics (CFD) model, can analyze solid-liquid two-phase flow, has also shown its potential in the field. This approach gives a comprehensive and detailed consideration to rheological properties of both particles and fluid. Its micro analysis of the interaction between solid and liquid has greatly improved the accuracy in calculations, depending on the correctness of the boundary conditions.

These two methods are not in any way related to each other. However, if they describe the physics correctly, they should certainly deliver the same results. Therefore, this study looks at the problem from two completely different points of view. The comparisons between the two methodologies can find out the disadvantages of these two methods in calculating the slurry transport process, and then help to work out their possible improvements.

2. Previous work

Based on a large amount of experimental data, Durand and Condolios (1952) have found that the hydraulic gradient of the heterogeneous slurry flow is related to the Froude number of the pipe flow. Later, by introducing the drag coefficient of the particles in the water, he has unified the experimental results of different particle sizes and put forward an empirical formula that has played a pioneering role. This formula has been used by the majority of the European dredging industry. Although in the further study, many researchers have found that the Durand's formula does not match the experimental results of others, it is still possible to obtain satisfactory results in the form of the formula by modifying the coefficients of the model. Newitt et al. (1955) have proposed a semi-empirical formula based on energy theory and gravity

* Corresponding author.
E-mail address: X.Chen-1@tudelft.nl (C. Xiuhan).

https://doi.org/10.1016/j.oceaneng.2019.03.065
Received 16 January 2018; Received in revised form 20 February 2019; Accepted 30 March 2019
Available online 13 April 2019
0029-8018/

theory. For heterogeneous flow, Newitt assumed that when the gravity particles continued to deposit, the additional pressure loss would be produced due to the potential energy used to sustain the particle suspension. In addition, he also obtained the critical flow rate formula based on the transition between sliding bed and heterogeneous flow. However, there are some objections to the theoretical part of this formula and it is not applicable to higher concentration. In Wasp's (1963) research, slurry consists of two parts, the fine particles and water as a carrier fluid, and the larger particles as transported particles according to Durand. The total resistance loss comprises two resistance losses from both the carrier and the larger particles. Wasp's model in the low velocity regime is as good as the model of Durand, and in the high velocity regime is as good as the equivalent liquid model. The model successfully integrates inhomogeneous and homogeneous flow regimes in one model, but it does not consider the possible presence of slip-bed phenomena in heterogeneous flow regimes. Wilson's (1979) two-layer model is based on force balance. His model theoretically assumes the following: the pipe is divided into the upper and lower layers, the concentration of particles in each layer is uniform and the flow velocity is the same. In the model, momentum transfer is calculated by the shear force at the interface. The model is widely used in sliding bed transportation. The model from Doron and Barnea (1993) is a two-layer model similar to the Wilson model, but the calculation is not accurate when there is a fixed bed at low flow rates. Hence, they have improved the two-layer model to a three-layer model. The two-layer model is still used for high velocity while at low flow rate, the second layer is subdivided into a fixed bed and a moving bed. Saskatchewan Research Council has proposed the SRC model and is updating the model over the years, starting from Shook and later continued by Gillies and Shook (2000). The theoretical basis behind the model remains unchanged in all versions. They assume that the particles causing Coulomb friction are in the lower layer while the other particles are fully suspended due to turbulence and evenly distributed in the pipe. The model contains many physical parameters, such as diameter, particle size and flow rate. This model is mainly used for the calculation of pressure drop and critical flow rate in the practice of coal transport. Kaushal et al. (2005) also applied the Wasp model, but with a modified concentration profile. Their predictions for concentration distribution have been confirmed to be in good agreement with the experimental data of the researchers. Subsequently, they modified the model by considering the effects of slurry concentration on particle diffusion. The new model can be used for the calculation of higher concentration slurry, and the obtained results are satisfactory.

Based on previous models and a large amount of experimental data, Miedema (2016) has put forward the DHLLDV Model according to physics. The model describes the main flow patterns (fixed bed flow, sliding bed flow, heterogeneous flow, pseudo-homogeneous flow and sliding flow) in slurry transportation. The advantages of the model lie in its wider applicability, its successful description of the above five-phase transition, and the excellent match of its calculations with corresponding experimental data.

Most models mentioned above are empirical or semi-empirical, combining the fundamental physics and experimental data. Dredging companies are interested in this kind of models. However, scientists are more interested in the internal structure and detailed development of the flow, which is also beneficial for further technology development.

With the help of the development of computer simulation technology, the CFD method becomes more and more popular in studying the multiphase flow problem. The CFD method allows scientists to get detailed internal structure of the flow. Ekambara et al. (2009) have adopted a three-dimensional numerical model based on particle flow dynamics, and made analysis on the sensitivity of flow field when imposed with different interphase force by using ANSYS-CFX. The simulation obtains good accuracy after both drag force and turbulent diffusive force are considered, whereas lift force and wall lubrication force have no significant influence on the calculation results. In addition, their research includes the effects of factors such as tube diameter (50–500 mm), slurry volume concentration (8–45%), particle size (90–500 μm), and mixture flow rate (1.5–5.5 m/s) on the concentration distribution. Kaushal et al. (2012) have used the Eulerian-Eulerian model and the mixture model respectively to simulate the flow of the fine and high-concentrated slurry particles in straight pipes. They have found that the Eulerian model predicts better results than the mixture model in terms of pressure drop, and that the error of the mixture model increases as the slurry concentration rises. Gopaliya and Kaushal (2015), after simulating the effects of particle size in the 53.2 mm pipe on pressure drop and concentration distribution, have found that with the particle size increasing, pressure drop per meter rises, and the largest concentration area climbs from the bottom of the pipe. kumar et al. (2016), also simulating the flow of slurry in 263 mm pipe diameter under different conditions, have found that the friction coefficient remained unchanged at the inlet section and the momentum transferring between particles and wall is strongly influenced by concentration and particle size, and the turbulent viscosity of slurry flow decreases with the increasing concentration. Messa and Malavasi, 2015 have used the Eulerian-Eulerian model to simulate the fully suspended solid-liquid slurry in a horizontal pipe. The particle shape is taken into account in calculating the viscosity of the mixture, and the software PHOENICS is used to solve the mathematical model. After calculated values are compared with the experimental data in the range of 90–640 μm(for particle size) and of 50–200 mm(for pipe diameter), the hydraulic gradient and the particle concentration distribution achieved good agreements.

In conclusion, the CFD method has promoted the further research of the granular pipe flow and has revealed the pipe flow details to the researchers, ensuring the accuracy of the key parameters for particle flows. At the same time, the existing empirical models not only have won better adaptability for being constantly revised and improved, but also wider application due to their convenience and computing speeds. In this study, the CFD model and the DHLLDV model are compared under different working conditions to evaluate their accuracy and adaptability, aiming to give guidance for further improvements in these two models.

3. Numerical model

3.1. The DHLLDV model

The DHLLDV Model created by Miedema (2017) is a new integrated model based on five main flow regimes: Fixed Bed, Sliding Bed, Heterogeneous transport, Homogeneous transport and Sliding Flow regime. The model describes all flow regimes in a consistent way showing the velocity transition between the flow regimes. This study chooses the heterogeneous transport and the homogeneous transport as the main flow regimes since these two are common in the dredging engineering.

3.1.1. Heterogeneous transport

This main flow regime behaves in a way that solids interact with the pipe wall through collisions. Solids are distributed non-uniformly over the cross section of the pipe with higher concentrations at the bottom of the pipe. This may be caused by saltation or by Brownian motions of the particles in turbulent transport.

The model in DHLLDV Model is based on the assumption that the excess hydraulic gradient is the result of energy losses, including potential energy losses and kinetic energy losses. The potential energy losses are dominated by the terminal settling velocity of the particles, as well as hindered settling. The kinetic energy losses are dominated by the ratio between the slip velocity of the particles and the terminal settling velocity of the particles. The pressure loss is shown in the equation with 3 independent terms. The viscous friction losses, the potential energy losses and the kinetic energy losses are as follows:

$$\Delta P_m = \Delta P_l + \Delta P_{s,pot} + \Delta P_{s,kin} = \Delta P_l \cdot (1 + \frac{\Delta P_{s,pot}}{\Delta P_l} + \frac{\Delta P_{s,kin}}{\Delta P_l}) \tag{1}$$

$$\Delta P_m = \Delta P_l \cdot (1 + \frac{\rho_l \cdot (\frac{V_t \cdot (1 - \frac{C_{vs}}{\kappa_c})^{\beta}}{V_{ls}}) \cdot g \cdot R_{sd} \cdot C_{vs}}{\lambda_l \cdot \frac{1}{D_p} \cdot \frac{1}{2} \cdot \rho_l \cdot V_{ls}^2} + \frac{\rho_l \cdot (\frac{V_{sl}}{V_t})^2 \cdot g \cdot R_{sd} \cdot C_{vs}}{\lambda_l \cdot \frac{1}{D_p} \cdot \frac{1}{2} \cdot \rho_l \cdot V_{ls}^2}) \tag{2}$$

The first item, ΔP_l, is the head loss of liquid over a pipeline length, and the second item$\Delta P_{s,pot}$, is the potential energy losses. The potential energy losses is proportional to the volumetric concentration C_{vs}, the submerged density of the solids R_{sd}, and the terminal settling velocity of the particles V_t, while inversely proportional to the line speed V_{ls}. The friction factor $\lambda_l$is influenced by the Reynolds number $R_e$of the flow in the pipe according to Moody diagram. The concentration eccentricity coefficient κ_c is in the range of 0.6–1, depending on the asymmetry of the concentration profile over the vertical in the pipe. The smaller this factor, the smaller the potential energy losses. β is the power index in the hindered settling equation of Richardson and Zaki (1954). The third item, $\Delta P_{s,kin}$, is the kinetic energy losses. The constant loss of kinetic energy is due to impact of the particles with the wall and also due to acceleration and deceleration in eddies. The slip velocity V_{ls} is defined as the difference between the average liquid velocity and the average particle velocity.

3.1.2. Homogeneous transport

The behavior of this main flow regime is, the particles are uniformly distributed over the cross section of the pipe due to the mixing capability of the turbulent flow. The pressure losses behave according to Darcy Weisbach, but with the mixture density as the liquid density. For very fine particles the viscosity has to be adjusted by the apparent viscosity.

In the case of very fine particles and/or very high line speeds, the liquid density often can be replaced by the mixture density in the hydraulic gradient equations. The velocity profile in a cross section of the pipe is considered to be symmetrical and the slip between the particles and the liquid is considered negligible. The concentration is assumed to be uniform over the cross section. This is often referred to as the equivalent liquid model (ELM). (Miedema, 2016)

$$\Delta P_m = \lambda_m \cdot \rho_m \cdot \frac{V_{ls}^2 \cdot \Delta L}{2 \cdot g \cdot D_p} \text{ with } \lambda_m = \lambda_l \tag{3}$$

But many researchers have found that, depending on the line speed and possibly some other parameters, there are certain deviations between the hydraulic gradient from the experiments and the ELM calculations. When particles are transported with relatively high line speeds, the hydraulic gradient from the experiments is below the value of ELM calculation, the near wall lift results in an almost particle free viscous sub-layer. However, in the case of very small particles with the Stokes number smaller than 0.03, the hydraulic gradient from the experiments is usually higher than the ELM calculation. The reason is that the very fine particles can move together with the liquid so that the apparent kinematic viscosity of the mixture has a significant increase.

Hence, Miedema proposed a ratio between the thicknesses of the viscous sublayer and the particle diameter δ_v/d (with a maximum of 1), combined with a concentration profile and then obtained a modified one — the RELM model, the equation is as follows:

$$\Delta P_m = \Delta P_l \cdot (1 + R_{sd} \cdot C_{vs} \cdot \frac{\delta_v}{d} + \frac{1 + R_{sd} \cdot C_{vs} - (A_{C_v} \cdot \ln(\frac{\rho_m}{\rho_l}) \cdot \sqrt{\frac{\lambda_l}{8}} + 1)^2}{(A_{C_v} \cdot \ln(\frac{\rho_m}{\rho_l}) \cdot \sqrt{\frac{\lambda_l}{8}} + 1)^2} \cdot (1 - \frac{\delta_v}{d})) \tag{4}$$

δ_v is the thickness viscous sub-layer, d is the diameter of the particle, A_{C_v} is the concentration factor, the A_{C_v} = 2.5–3 by the latest calibration tests.

3.2. The CFD model

Euler-Euler multiphase model is used to simulate the fully-suspended flow in a way that different phases are treated mathematically as interpenetrating continua. The fundamental equations of mass, momentum, and energy conservation are then solved for each phase. The coupling of both phases is achieved through pressure and interphase exchange coefficients. The model uses granular kinetic theory to describe interaction between particles, and considers interfacial forces such as the drag force caused by the difference of phase speeds, the virtual mass force due to particle acceleration, the lift force due to phase velocity gradient, and other forces.

3.2.1. Conservation equations

(1) Continuity Equation

Each phase is described by making use of volume-averaged, incompressible, transient Navier-Stokes equations.

$$\frac{\partial}{\partial t}(\alpha_l \rho_l) + \nabla \cdot (\alpha_l \rho_l \vec{v_l}) = 0 \tag{5}$$

$$\frac{\partial}{\partial t}(\alpha_s \rho_s) + \nabla \cdot (\alpha_s \rho_s \vec{v_s}) = 0 \tag{6}$$

where α is the concentration of each phase, l is the liquid phase, s is the particle phase, ρ is the density, and v is the phase velocity.

(2) Momentum Equation

The momentum balance for the liquid phase is modified based on the Navier-Stokes equation, including an interphase momentum transfer term.

$$\frac{\partial}{\partial t}(\alpha_l \rho_l \vec{v_l}) + \nabla \cdot (\alpha_l \rho_l \vec{v_l} \vec{v_l}) = -\alpha_l \nabla p + \nabla \cdot \bar{\bar{\tau}}_l + \alpha_l \rho_l \vec{g} + F_k \tag{7}$$

$$\frac{\partial}{\partial t}(\alpha_s \rho_s \vec{v_s}) + \nabla \cdot (\alpha_s \rho_s \vec{v_s} \vec{v_s}) = -\alpha_s \nabla p + \nabla \cdot \bar{\bar{\tau}}_s + \alpha_s \rho_s \vec{g} - \alpha_s \nabla p_s + F_k \tag{8}$$

The $\bar{\bar{\tau}}_l$ and $\bar{\bar{\tau}}_s$ are the shear stress tensors of the liquid phase and the solid phase respectively. The F_k is the sum of the interface forces, including drag force F_d, lift force F_l, virtual mass force F_{vm} and turbulent diffusive forces F_{td}.

The drag force is given by:

$$F_d = K_{sl}(\vec{v_s} - \vec{v_l}) \tag{9}$$

$K_{sl}$is the fluid-solid momentum exchange coefficient given by Gidaspow model, when $\alpha_l > 0.8$,

$$K_{sl} = \frac{3}{4} C_d \frac{\alpha_s \alpha_l \rho_l |\vec{v_s} - \vec{v_l}|}{d_s} \alpha_l^{-2.65} \tag{10}$$

where $C_d$is the drag coefficient given by:

$$C_d = \frac{24}{\alpha_s Re_s}[1 + 0.15(\alpha_l Re_s)^{0.687}] \tag{11}$$

$$Re_s = \frac{\alpha_l \rho_l d_s |\vec{v_s} - \vec{v_l}|}{\mu_l} \tag{12}$$

when $\alpha_l \leq 0.8$,

$$K_{sl} = 150 \frac{(1 - \alpha_l)^2 \mu_l}{\alpha_l d_s^2} + 1.75 \frac{\rho_l (1 - \alpha_l) |\vec{v_s} - \vec{v_l}|}{d_s} \tag{13}$$

The lift force is given by Drew model:

$$F_l = C_l \alpha_s \rho_l (\vec{v_l} - \vec{v_s}) \times (\nabla \times \vec{v_l}) \tag{14}$$

where C_l is the lift coefficient taken as 0.5 (Default value).

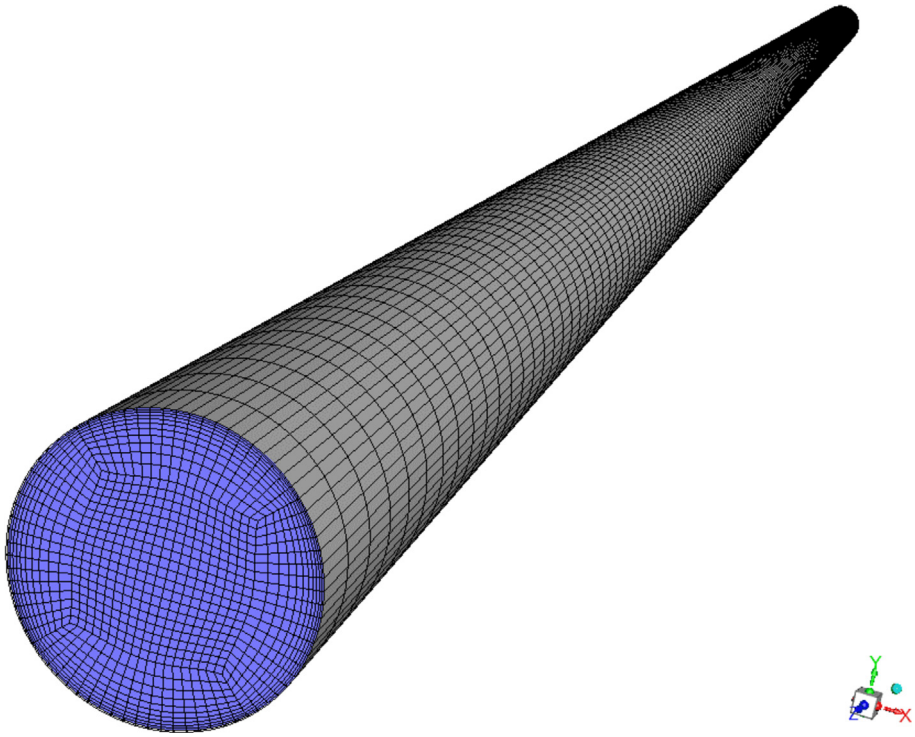

Fig. 1. Physical model and mesh.

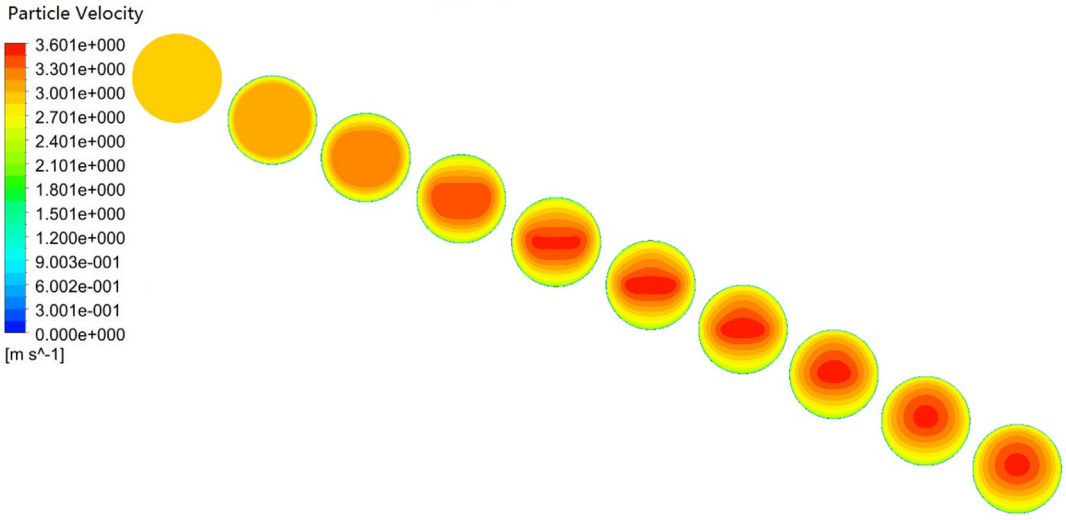

Fig. 2. Velocity distribution in pipe cross section along the flow direction.

The virtual mass force $F_{vm}$is given by:

$$F_{vm} = C_{vm}\alpha_s\rho_l(d_l\vec{v}_l/d_t - d_s\vec{v}_s/d_t) \tag{15}$$

where $C_{vm}$is the virtual mass coefficient which typically has a value of 0.5.

The turbulent dispersion force is given by Burns et al. model:

$$F_{td} = C_{td}K_{sl}D_l/\sigma_{sl}(\nabla\alpha_s/\alpha_s - \nabla\alpha_l/\alpha_l) \tag{16}$$

where $C_{td}$is the coefficient of turbulent diffusive forces. $C_{td} = 1$ and $\sigma_{sl} = 0.9$ (Default value), and the dispersion scalar is estimated by the turbulent viscosity of the continuous phase: $D_l = D_s = D_{sl} = \frac{\mu_{tl}}{\rho_l}$

3.2.2. Granular temperature equation

The kinetic theory used in this model is very critical in that it accounts for the effects of the interactions between the solid phase and the liquid phase. The stress is defined as function of granular temperature Θ_s, which represents particle velocity fluctuations and is proportional to the mean square of the random motion of particles. Granular temperature is solved using the following transport equation:

$$\frac{3}{2}[\frac{\partial}{\partial t}(\rho_s\alpha_s\Theta_s) + \nabla\cdot(\rho_s\alpha_s\vec{v}_s\Theta_s)] = (-p_s\overline{\overline{I}} + \overline{\overline{\tau}}_s)\colon\nabla\vec{v}_s + \nabla\cdot\left(k_{\Theta_s}\nabla\Theta_s\right) - \gamma_{\Theta_s} + \phi_{ls} \tag{17}$$

The left-hand side of this equation represents the net change of fluctuating energy. The first term on the right-hand side represents the fluctuating energy due to solids pressure and viscous forces. The second term is the diffusion of fluctuating energy in the solids phase. γ_{Θ_s}represents the dissipation of fluctuating energy and γ_{Θ_s} is the exchange of fluctuating energy between the liquid and solids phase.k_{Θ_s} is the diffusion coefficient provided by Gidaspow.

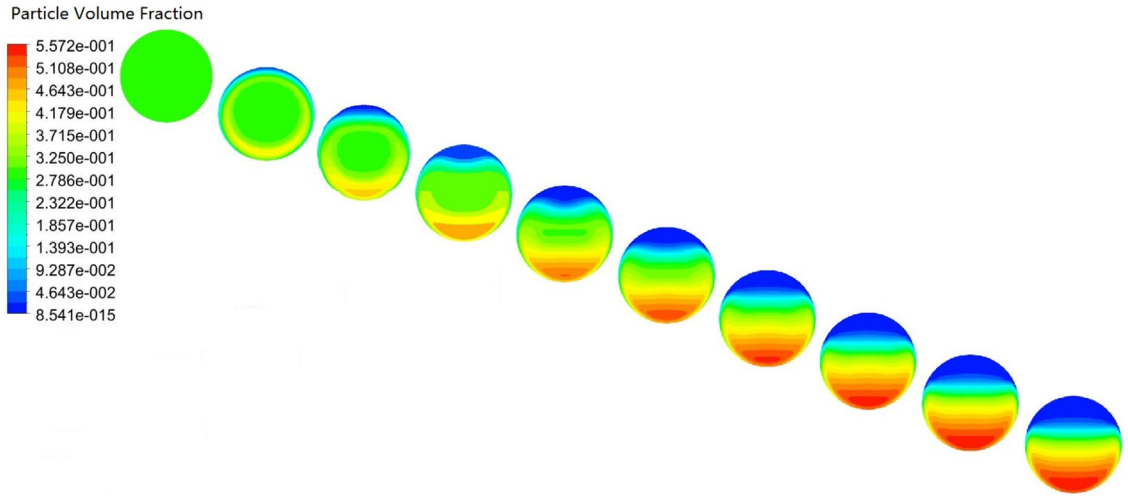

Fig. 3. Concentration distribution in pipe cross section along the flow direction.

Table 1
Five groups of experiment parameters.

ID	D/(mm)	d_p/(μm)	ρ_s/(kg/m^3)	V_m/(m/s)	C_v/(%)	Researcher
P1	53	100	2440	2–5	15–30	Schaan et al. (2000)
P2	54.9	125	2470	1–5	20	Kaushal et al. (2005)
P3	103	90	2650	3–7	19–33	Gillies et al. (2010)
P4	150	370	2650	4–9	26	Matousek (2002)
P5	54.9	440	2470	1–5	20–30	Kaushal et al. (2005)

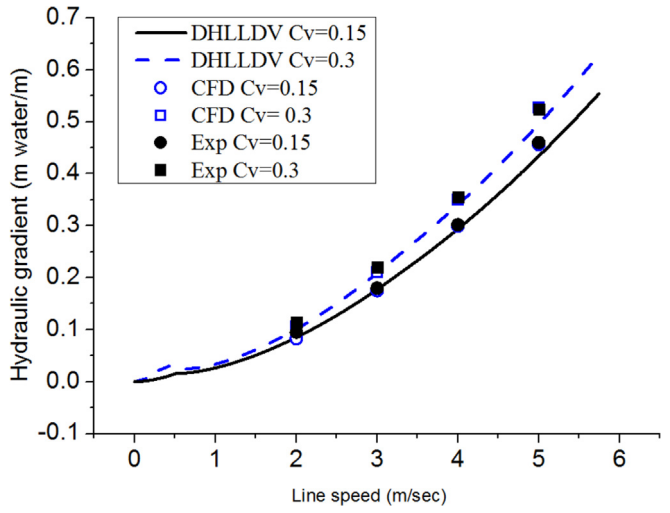

Fig. 4. Comparative Analysis of Hydraulic Gradient (D = 53 mm, dp = 100 μm, Cv = 0.15–0.3).

$$k_{\Theta_s} = \frac{150\rho_s d_s\sqrt{\Theta_s\pi}}{384(1+e_{ss})g_{0,ss}}[1+\frac{6}{5}\alpha_s g_{0,ss}(1+e_{ss})]^2 + 2\rho_s\alpha_s^2 d_s(1+e_{ss})g_{0,ss}\sqrt{\frac{\Theta_s}{\pi}} \quad (18)$$

The dissipation fluctuating energy is

$$\gamma_{\Theta_s} = \frac{12(1-e_{ss}^2)g_{0,ss}}{d_s\sqrt{\pi}}\rho_s\alpha_s^2\Theta_s^{\frac{3}{2}} \quad (19)$$

Here e_{ss} is the coefficient of restitution for particle collisions, used to quantify the elasticity of particle collisions (one for fully elastic and zero for the fully inelastic), and taken as 0.9. d_s is the particle diameter. $g_{0,ss}$ is the radial distribution function at contact, and is interpreted as the probability of particle touching another particle:

$$g_{0,ss} = [1-(\frac{\alpha_s}{\alpha_{s,max}})^{\frac{1}{3}}]^{-1} \quad (20)$$

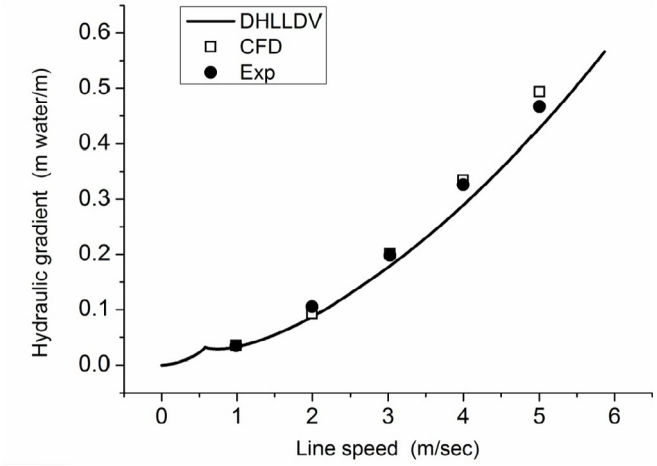

Fig. 5. Comparative Analysis of Hydraulic Gradient (D = 55 mm, dp = 125 μm, Cv = 0.2).

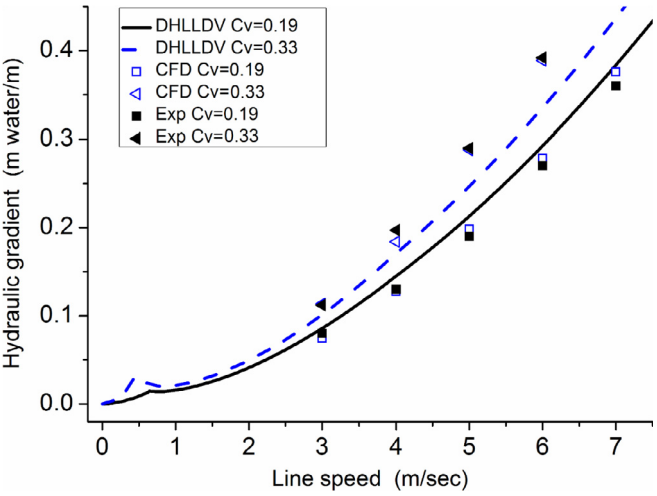

Fig. 6. Comparative Analysis of Hydraulic Gradient (D = 103 mm, dp = 90 μm, Cv = 0.19–0.33).

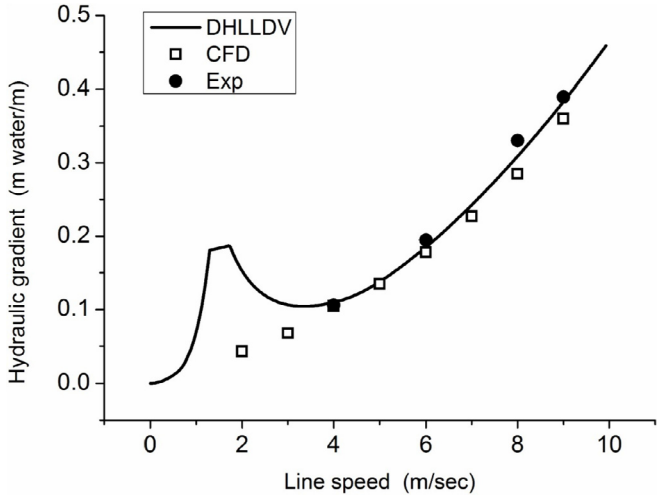

Fig. 7. Comparative Analysis of Hydraulic Gradient (D = 150 mm, dp = 370 μm, Cv = 0.26).

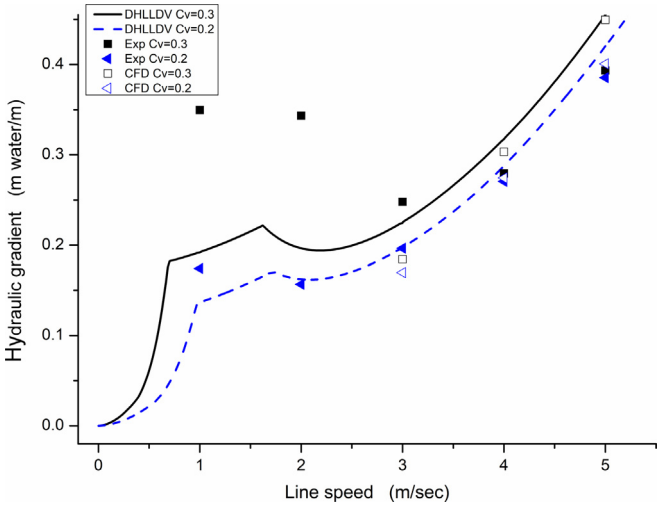

Fig. 8. Comparative Analysis of Hydraulic Gradient (D = 54.9 mm, dp = 440 μm, Cv = 0.2–0.3).

where $\alpha_{s,max}$is the static settled concentration put as 0.63.

The shear viscosity of the solid is given as:

$$\mu_s = \mu_{s,col} + \mu_{s,kin} + \mu_{s,fr} \tag{21}$$

Where, $\mu_{s,col}$, $\mu_{s,kin}$ and $\mu_{s,fr}$ are the collisional, kinetic and frictional viscosities and are calculated respectively using the following equations:

$$\mu_{s,col} = \frac{4}{5}\alpha_s\rho_s d_s g_{0,ss}(1+e_{ss})\left(\frac{\Theta_s}{\pi}\right)^{\frac{1}{2}}\alpha_s \tag{22}$$

$$\mu_{s,kin} = \frac{10\rho_s d_s\sqrt{\Theta_s\pi}}{96\alpha_s(1+e_{ss})g_{0,ss}}\left[1+\frac{4}{5}g_{0,ss}\alpha_s(1+e_{ss})\right]^2\alpha_s \tag{23}$$

$$\mu_{s,fr} = \frac{p_s\sin\phi}{2\sqrt{I_{2D}}} \tag{24}$$

The solid bulk viscosity has the form from Lun et al.model:

$$\lambda_s = \frac{4}{3}\alpha_s\rho_s d_s g_{0,ss}(1+e_{ss})\left(\frac{\Theta_s}{\pi}\right)^{\frac{1}{2}} \tag{25}$$

where π is circumference ratio; $d_s$is the particle diameter; $e_{ss}$is the restitution coefficient, taken as 0.9.

3.2.3. Turbulence equations

Turbulence in liquid phase and solid phase, considered as mixture phase, is simulated through the mixture turbulence model, an extension model of the single-phase k-ε model. The turbulence equation is given as follows:

$$\frac{\partial(\rho_m k)}{\partial t} + \frac{\partial(\rho_m \overrightarrow{v_m} k)}{\partial x_i} = \frac{\partial}{\partial x_i}\left[(\mu_m + \frac{\mu_{t,m}}{\sigma_k})\frac{\partial k}{\partial x_i}\right] + G_{k,m} - \rho_m\varepsilon \tag{26}$$

$$\frac{\partial(\rho_m \varepsilon)}{\partial t} + \frac{\partial(\rho_m \overrightarrow{v_m}\varepsilon)}{\partial x_i} = \frac{\partial}{\partial x_i}\left[(\mu_m + \frac{\mu_{t,m}}{\sigma_\varepsilon})\frac{\partial \varepsilon}{\partial x_i}\right] + \frac{\varepsilon}{k}(C_{1\varepsilon}G_{k,m} - C_{2\varepsilon}\rho_m\varepsilon)\frac{\varepsilon^2}{k} \tag{27}$$

In these equations, μ_{tm}represents the turbulent viscosity of the mixture, $G_k$represents the generation of turbulent kinetic energy due to the mean velocity gradient.

$$\mu_{t,m} = \rho_m C_\mu \frac{k^2}{\varepsilon} \tag{28}$$

$$G_{k,m} = \mu_{t,m}[\nabla\overrightarrow{v_m} + (\nabla\overrightarrow{v_m})^T]\colon\nabla\overrightarrow{v_m} \tag{29}$$

As the default, $\sigma_k = 1.0$, $\sigma_\varepsilon = 1.3$, $C_\mu = 0.09$, $C_{1\varepsilon} = 1.44$ and $C_{2\varepsilon} = 1.92$.

4. Numerical simulation

4.1. Physical model and mesh

For comparison with existing experimental data, this study has established several models of horizontal pipes with a variety of inner diameters D and lengths (L = 50D). To ensure good accuracy in computations and to achieve convergence, 20 exponential boundary layers are established along the wall with a growth factor of 1.2(each row of the boundary layer mesh is 20% thicker than the previous row), and the height of the outermost layer is approximately 2 mm. Moreover, the height of the first layer from the wall is expressed as a dimensionless parameter, y+, where y+ < 30. The total number of cells in each of these 3D models is approximately 300,000, as shown in Fig. 1.

4.2. Boundary conditions

The velocity-inlet condition is provided at the inlet. Specified values are assigned to the velocities and concentrations of both phases. The pressure-outlet condition with atmospheric pressure is applied at the outlet.

Roughness height has a large effect on the pressure calculation. It is taken as 0.2 mm according to the pipe materials. The no-slip boundary condition is used in the liquid phase. The Johnson and Jackson (1987) partial slip boundary conditions are used in the solid phase to determine the tangential velocity and the particle temperature of the solid phase at the wall. Johnson and Jackson have assumed that some particles continue to slip at the wall while other particles collide with each other. The particle-wall specularity coefficient φ represents the loss of tangential momentum at the collision between the particle and the wall. φ is set as 0.05 in the previous calculation, in view of its relation to the pipe wall roughness and of its value range from 0 to 1.

4.3. Solving process and convergence schemes

A CFD software FLUENT 16.1 has been adopted to simulate the slurry flow through prescribed boundary conditions and turbulence model. The finite volume method is used to discretize the basic governing equations of liquid-solid two-phase flow. The pressure-based separation algorithm is adopted to solve the conservation equations, and the SIMPLE (Patankar & Spalding, 1972) algorithm is used to realize the coupling of pressure field and velocity field. In order to achieve stable calculation and quick solution, the momentum equation

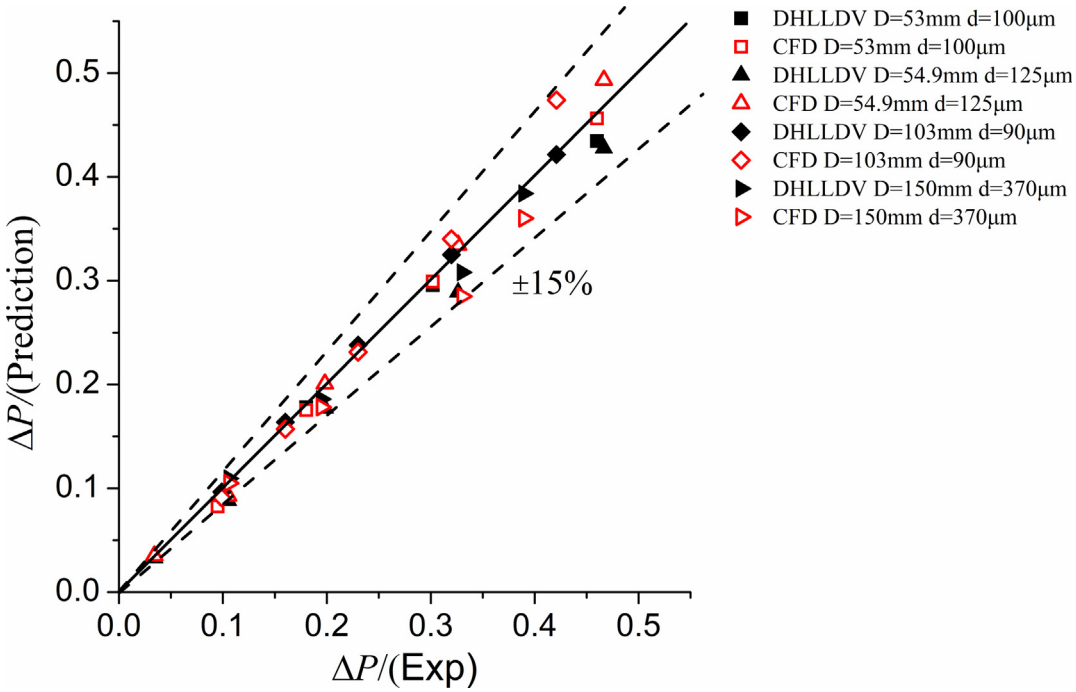

Fig. 9. Comparative error analysis of CFD and DHLLDV Model.

Table 2
Six groups of experiment parameters.

ID	d_p/(μm)	D/(mm)	ρ/(kg/m^3)	V_m/(m/s)	C_v/(%)	Researcher
A1	90	103	2650	3.00	19	Gillies
A2	90	103	2650	3.00	24	Gillies
A3	90	103	2650	3.00	29	Gillies
A4	90	103	2650	3.00	33	Gillies
B1	165	51.5	2650	3.78	9	Roco&Shook
B2	165	51.5	2650	4.17	19	Roco&Shook
B3	165	51.5	2650	4.33	29	Roco&Shook
C1	165	263	2650	3.50	9.95	Roco&Shook
C2	165	263	2650	3.50	18.4	Roco&Shook
C3	165	263	2650	3.50	26.8	Roco&Shook
C4	165	263	2650	3.50	33.8	Roco&Shook
D1	270	103	2650	5.40	10	Gillies
D2	270	103	2650	5.40	20	Gillies
D3	270	103	2650	5.40	30	Gillies
D4	270	103	2650	5.40	40	Gillies
E1	370	150	2650	5.99	26	Matousek
E2	370	150	2650	5.99	35	Matousek
F1	440	54.9	2470	3.00	9.39	Kaushal
F2	440	54.9	2470	3.00	21.68	Kaushal
F3	440	54.9	2470	3.00	30.01	Kaushal
F4	440	54.9	2470	3.00	41.59	Kaushal

adopts QUICK (Hayase et al., 1992) discretization algorithm, the volume fraction equation adopts the second-order upwind scheme, and the other control equations adopt the first-order upwind scheme. The time step is 0.001s. Root mean square residuals are used, and the residuals for convergence are set equal to 10^{-5}.

5. Analysis and discussion

The CFD and DHLLDV calculations have been carried out to match a wide range of experimental conditions for fully suspended flow. Then the hydraulic gradient and concentration distribution are compared respectively.

5.1. Flow stability analysis

The paper first analyzes the particle flow along the pipeline. It chooses slurry with particle size d_p = 440 μm and volume concentration C_v = 30%, and being delivered at an average velocity of V_m = 3 m/s, to study how the flow regimes change in the pipeline. In each of Fig. 2 and Fig. 3, ten sections of flow field cloud are taken from inlet to outlet at 5D intervals.

As shown in Fig. 2, particles will have higher velocity near the center of the pipe, and lower velocity at the wall, because the carrier fluid has zero velocity at the wall and strong shear in the turbulent boundary layer. As Fig. 3 shows. the slurry concentration in the pipe gradually shows a gradient with the flow of slurry, decreasing at the upper part of the pipe and increasing at the lower part. In the high concentration area of the lower part of the pipeline, the carrier fluid needs to consume more energy to move the particles, while the upper particles are weaker due to the mutual flow, and the maximum velocity center gradually moves to the pipeline. With the development of fluid flow, the particle distribution remains unchanged. The maximum particle flow velocity is constant and the peak velocity region remains unchanged.

From the above analysis, it can be seen that the slurry flow before 40D is the developing flow in the inlet section, and the fluid flow of the slurry fluid changes gradually with the flow. After 40D, the fully developed turbulent flow remains stable. In order to assure the reliability of the numerical results analysis, in the later simulation, the section of the selected cloud is 50D, and the characteristic curve takes the value of the vertical centerline of the 50D cross section.

5.2. Hydraulic gradient

The hydraulic gradient, showing the pipeline pressure loss, is an important parameter in slurry pipeline transportation and determines the energy consumption of slurry pump. Therefore, the hydraulic gradients calculated by both CFD and DHLLDV models are made comparative analysis with experiment data of Schaan et al. (2000); Kaushal et al. (2005); Gillies et al. (2010) and Matousek (2002), so as to verify these two models. The parameters are shown on Table 1.

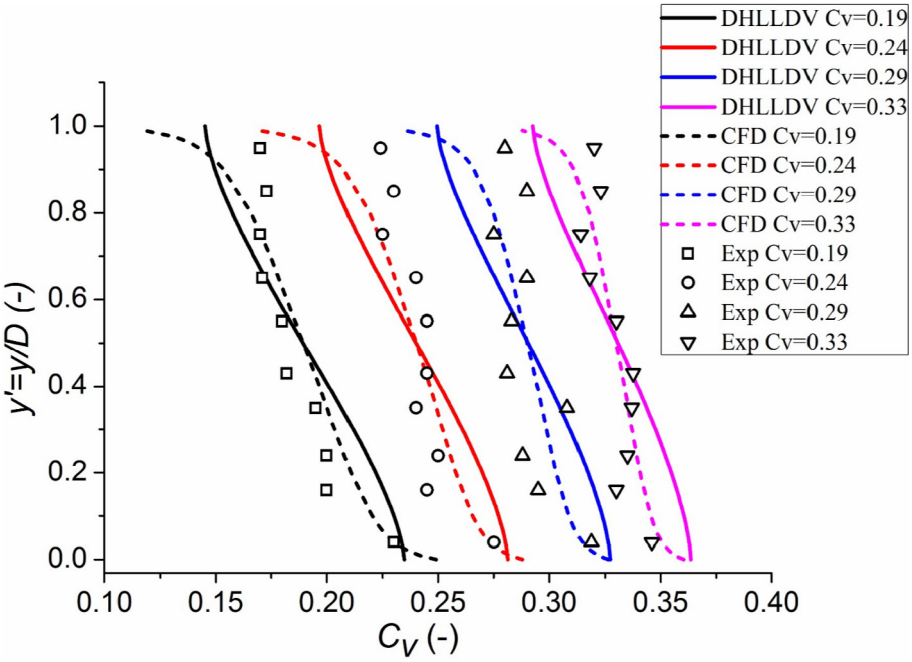

Fig. 10a. Comparative analysis of concentration distribution (dp = 90 μm, D = 103 mm, V = 3 m/s).

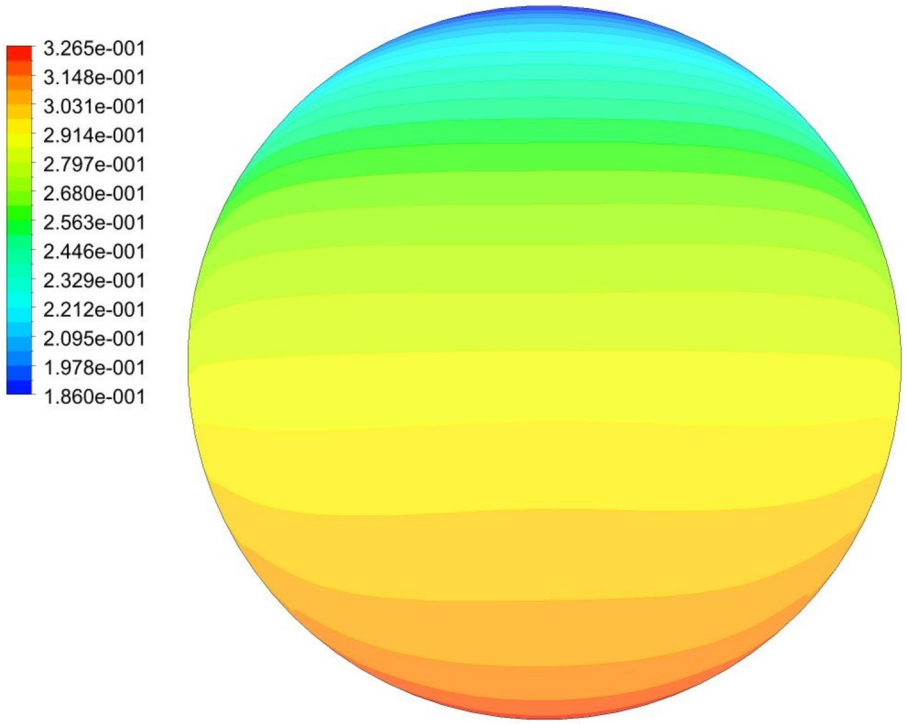

Fig. 10b. The concentration contour (C_v = 0.29, dp = 90 μm, D = 103 mm, V = 3 m/s).

The hydraulic gradient calculation results shown in Figs. 4–9. It can be seen from Figs. 4–5 that the hydraulic gradient almost increases with the pace of the slurry velocity, the flow regime is the fully-suspended flow, and the main pressure losses are caused by viscous friction losses, the potential energy losses and the kinetic energy losses. When the slurry line speed is less than 1 m/s, a little inflection point will appear in the DHLLDV curve. At that time when the flow regime of slurry transfers to the fixed-bed flow, the liquid has to flow through a restricted area above the bed, resulting in higher pressure losses. The hydraulic gradient experiment data are in good agreement with the CFD and DHLLDV data.

Fig. 6 shows the hydraulic gradient curve when the pipe diameter increases to 103 mm. The calculation results of DHLLDV slightly deviate from the experimental data with the increasing of slurry concentration and velocity. Because the particle movement with its increasing concentration and velocity strengthens the influence on hydraulic gradient, the calculation from equation (4) may have certain deviation.

When the pipe diameter increases to 150 mm and the particle diameter increases to 370 μm, the result can be seen from Fig. 7. The calculated pressure data of CFD and DHLLDV agree well with the

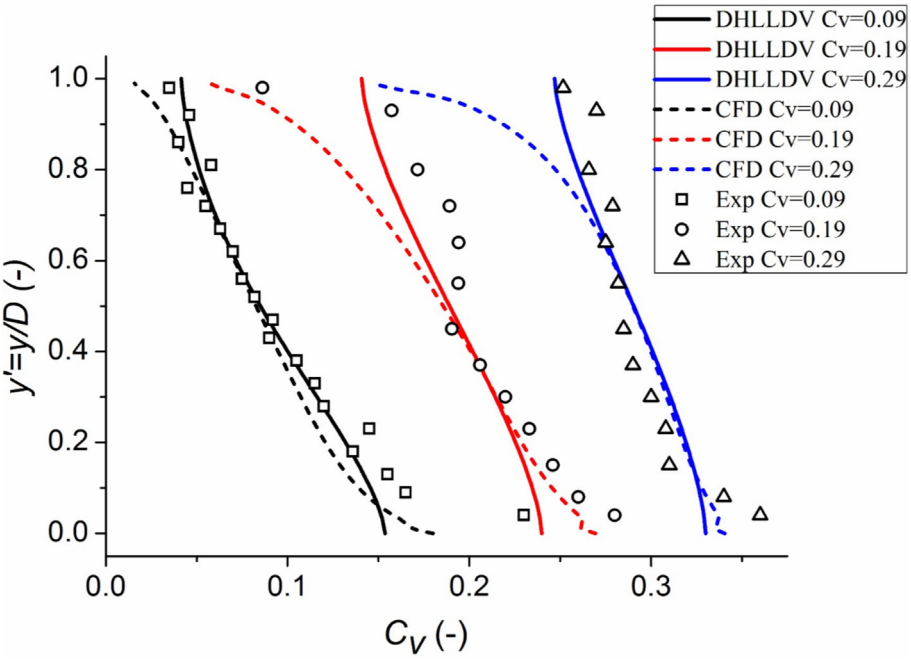

Fig. 11a. Comparative analysis of concentration distribution (dp = 165 μm, D = 51.5 mm, V = 3.78–4.33 m/s).

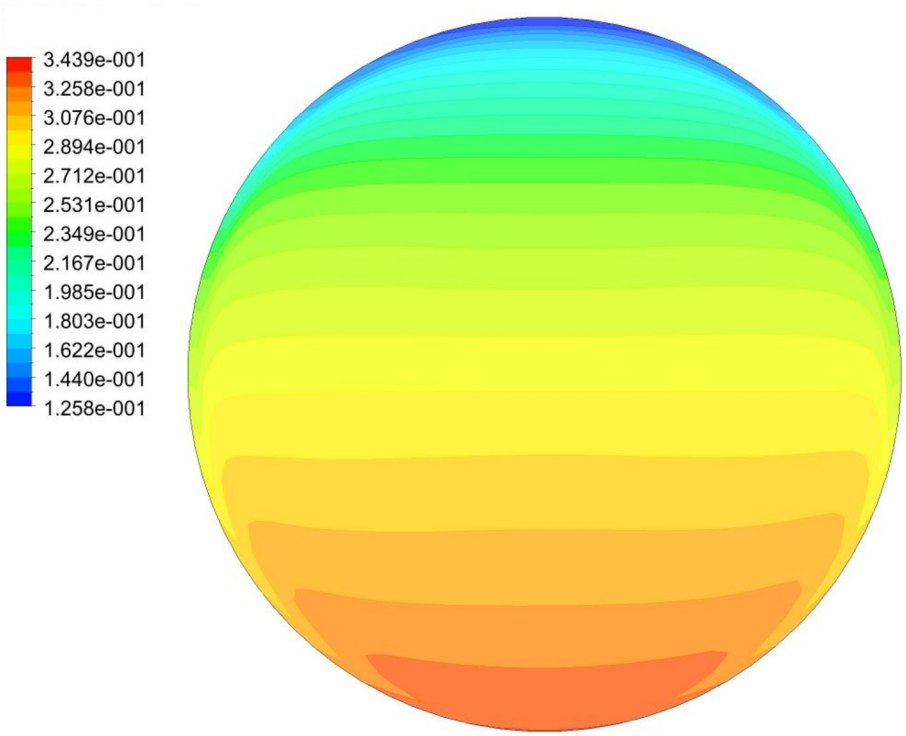

Fig. 11b. The concentration contour (C_v = 0.29, dp = 165 μm, D = 51.5 mm, V = 4.33 m/s).

experimental data at the slurry speed of 4–10 m/s. When the velocity is lower than 4 m/s, deviation happens to both the CFD and DHLLDV calculations, possibly due to changes in slurry flow regimes. The CFD model shows not very obvious transition in flow regimes when slurry velocity is below critical velocity, so the hydraulic gradient curve is still similar to that of fully-suspended flow regime.

To have a further research in calculations of how larger particles flow at low velocities, this paper has chosen the experiment data of Kausual et al. (2005) for comparative analysis with the particle diameter at 440 μm, slurry concentration respectively at 20% and 30%, and velocity ranging from 1 m/s to 5 m/s, as shown in Fig. 8. From the comparison between CFD and DHLLDV model and test data. A reversal appears in the hydraulic gradient curve both of DHLLDV and test data, because the particle settling becomes dominant with the increasing of particle diameter and decreasing of line velocity. When the slurry velocity is below critical velocity, the flow regime of slurry will transfer from fully-suspended flow to the sliding bed flow and then to the fix-bed flow. The pressure losses at the moment are mainly caused by the sliding friction of the solids and the viscous friction of the liquid. The DHLLDV chooses for each flow regime the corresponding empirical

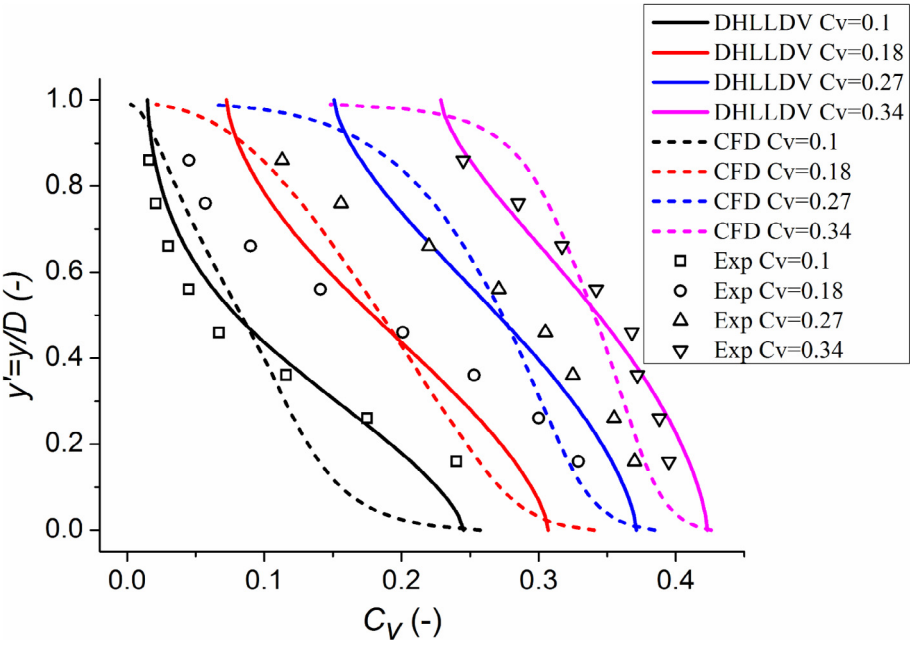

Fig. 12a. Comparative analysis of concentration distribution (dp = 165 μm, D = 263 mm, V = 3.5 m/s).

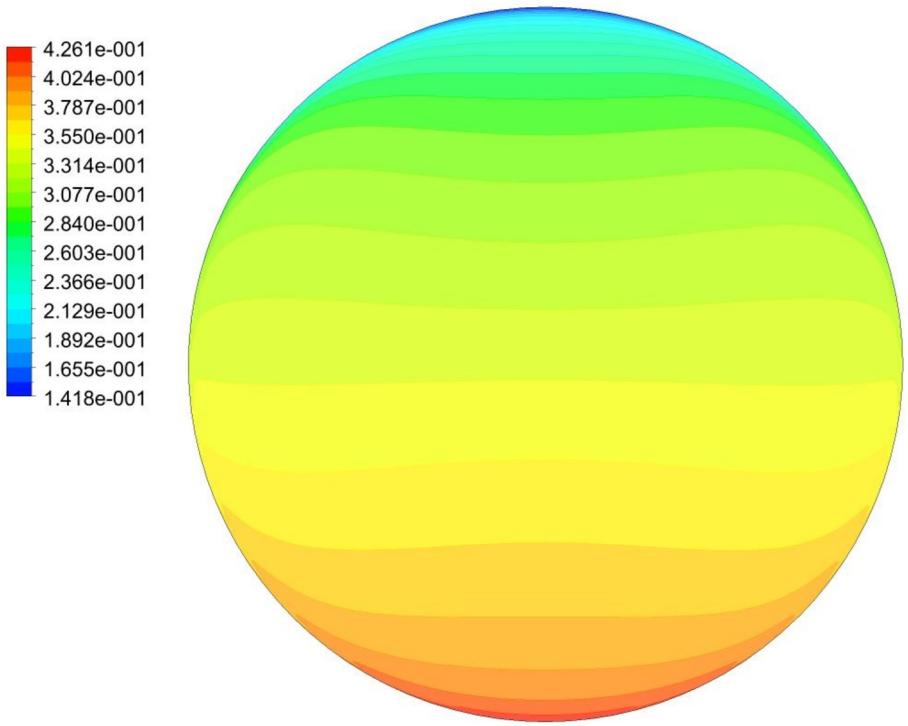

Fig. 12b. The concentration contour (C_v = 0.338, dp = 165 μm, D = 263 mm, V = 3.5 m/s).

equation to make piecewise solution, so the trend of curve is reversed. When concentration is at 20%, the calculation results from DHLLDV are in good match with experiment data. When the concentration is at 30%, deviation happens when velocity is less than 2 m/s. There are good matches between CFD calculations and experiment data when the velocity is 3–5 m/s. When the velocity is below the critical one, however, particle settling escalates and Euler-Euler model cannot apply to the flow regime, resulting in divergent results.

Besides, for all the cases of above critical velocity, test data of 4 different diameters are compared with the calculated data. It can be seen from Fig. 9 that the predictions of hydraulic gradient in both CFD and DHLLDV calculations are accurate in the sense of errors within 15%. Therefore, both methods are feasible to predict the hydraulic gradient of fully-suspended slurry flow.

5.3. Concentration distribution

21 groups of experimental conditions taken from Gillies et al. (2010); Roco & Shook (1983); Matousek (2002) and Kaushal et al. (2005), including diameter of pipeline D = 51.5–263 mm, particle size d_p = 90–440 μm and volume concentration of slurry C_v = 9%–41.59% were selected to analyze the concentration distribution. The main

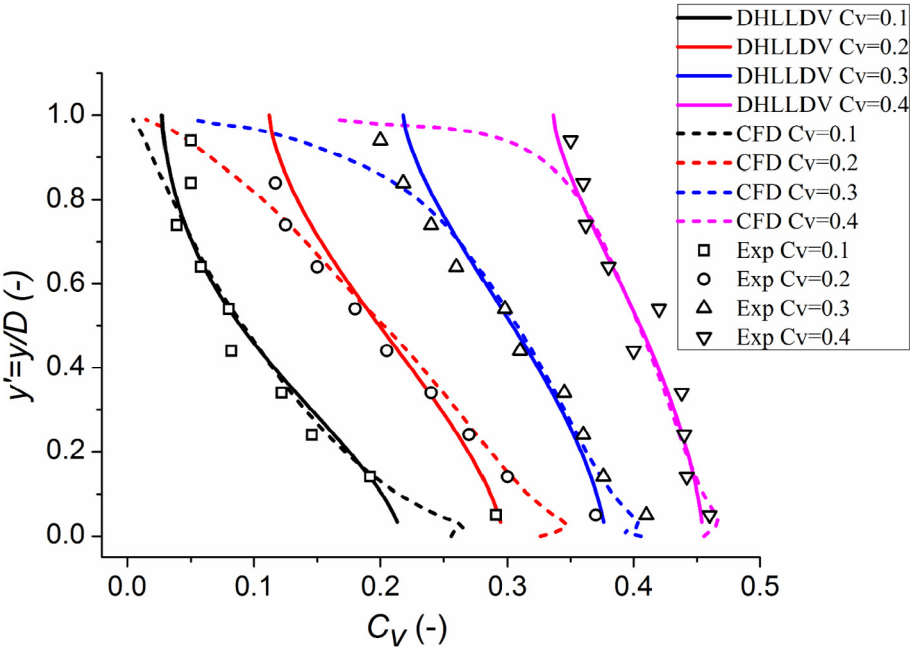

Fig. 13a. Comparative analysis of concentration distribution (dp = 270 μm, D = 103 mm, V = 5.4 m/s).

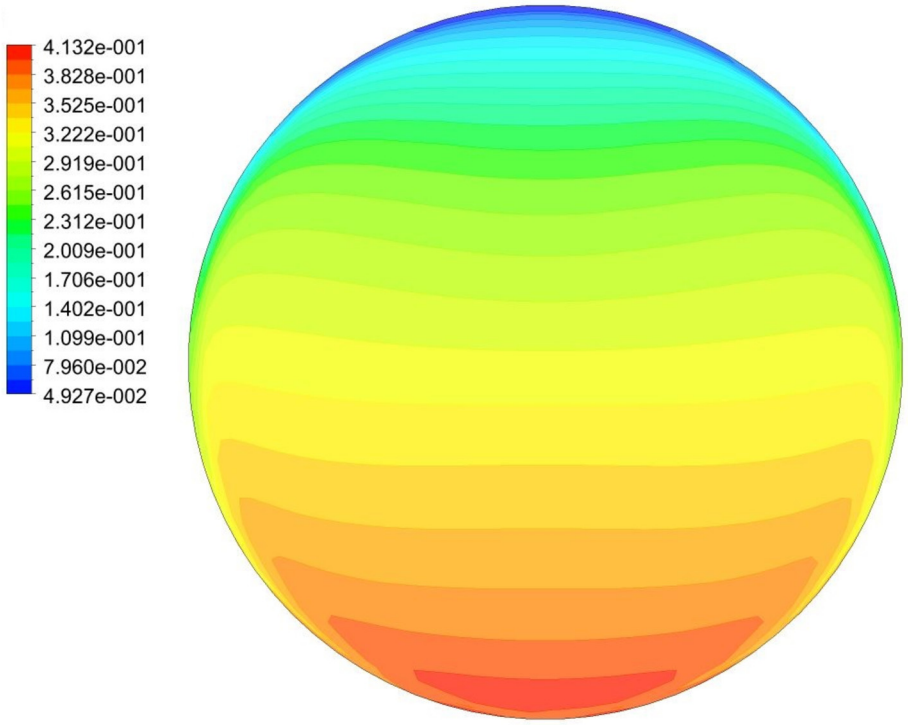

Fig. 13b. The concentration contour (C_v = 0.3, dp = 270 μm, D = 103 mm, V = 3.5 m/s).

parameters of each experimental conditions are shown in Table 2.

The concentration distribution calculation results are shown in Figs. 10–15.

Figs. 10–15 shows the comparisons between the simulated results and the experimental data in the particle volume fraction on the vertical center line of the pipe cross-section under different conditions. It can be seen from the figures that the simulation results of various working conditions with different pipe diameters have good agreement with the corresponding experimental data except Fig. 15. Especially in the central part of the pipe, both CFD and DHLLDV show good consistency. However, there is a certain deviation between two calculated values and the experimental values in the upper and lower parts of the pipeline, and the two curves show different trends of near-wall concentration distribution.

These may come from the following reasons. For one thing, the tested data of near-wall concentration may not be accurate. A similar phenomenon has also been reported by Gopaliya & Kaushal (2015). For another, errors may occur because of the simplification of CFD and DHLLDV in calculating near-wall concentration.

In the CFD model, the flow of turbulent core area is solved by the turbulent equations, while the flow of near-wall area (viscous sublayer and transition layer) is solved by the semi-empirical equations i.e. the

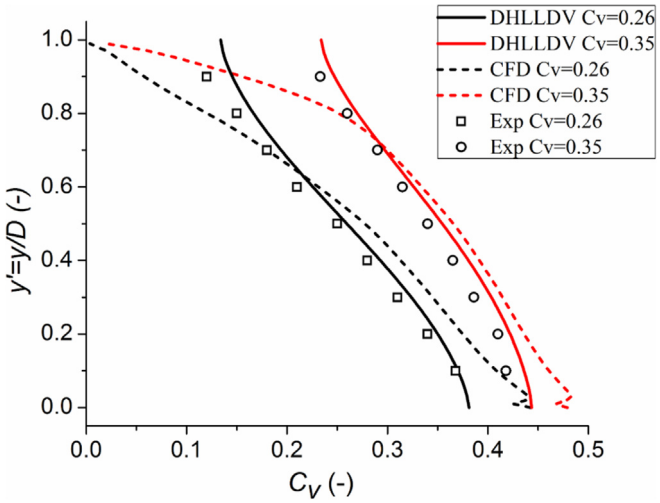

Fig. 14a. Comparative analysis of concentration distribution (dp = 370 μm, D = 150 mm, V = 5.99 m/s).

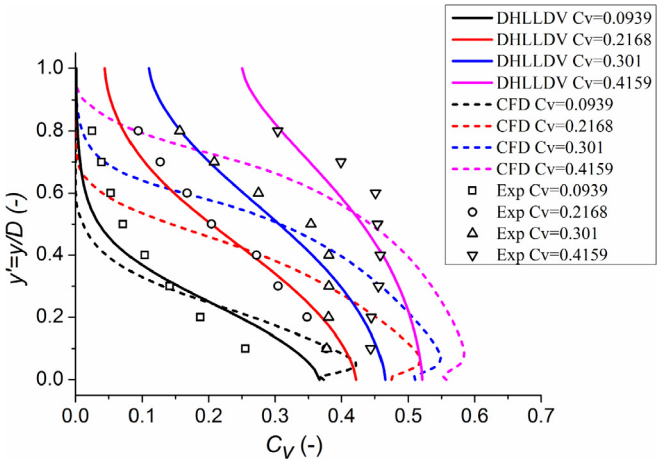

Fig. 15a. Comparative analysis of concentration distribution (dp = 440 μm, D = 54.9 mm, V = 3 m/s).

wall functions. However, if the wall condition cannot be selected correctly according to the real flow, deviation still happens to the CFD model. DHLLDV model with its concentration calculations based on advection-diffusion equation, has modified the diffusion coefficient, and also calculated the concentration distribution over the cross section of the pipe from the bottom to the top with the bottom concentration as the reference point. This model replaces the vertical coordinate r/D_p with the fraction of the cross section f so that it can better calculate the average concentration in the cross sections. Meanwhile, this model, taking the Limit Deposit Velocity (LDV) effect into consideration, treats the ratio between the line speed and the LDV as an influential parameter for concentration distribution to improve the accuracy. When particles have irregular movements in the near-wall area owing to different forces, error will occur in the calculation of concentration distribution.

To further explain this problem, it should be pointed out that the concentration distribution is often calculated based on the advection-diffusion equation. In this equation the downwards transport flux of the solids at a certain location in the pipe equals the hindered settling velocity times the local concentration. The upwards transport flux of the solids equals the concentration gradient times the diffusivity. The diffusivities here cover both the turbulence diffusivity and momentum diffusivity. In a stationary situation the upwards solid flux + the downwards solid flux equals zero, so no net solid flux in any direction. It is often assumed that the diffusivity for particle momentum is equal to the turbulent diffusivity. Many analytical solutions are based on a constant diffusivity, and also a calculated cross sectional averaged hindered settling velocity, by using the average volumetric concentration in the pipe.

Some of the assumptions in the above approach are questionable. In reality the turbulent diffusivity is not a constant in a pipe but will be larger in the center of the pipe and smaller close to the pipe wall.

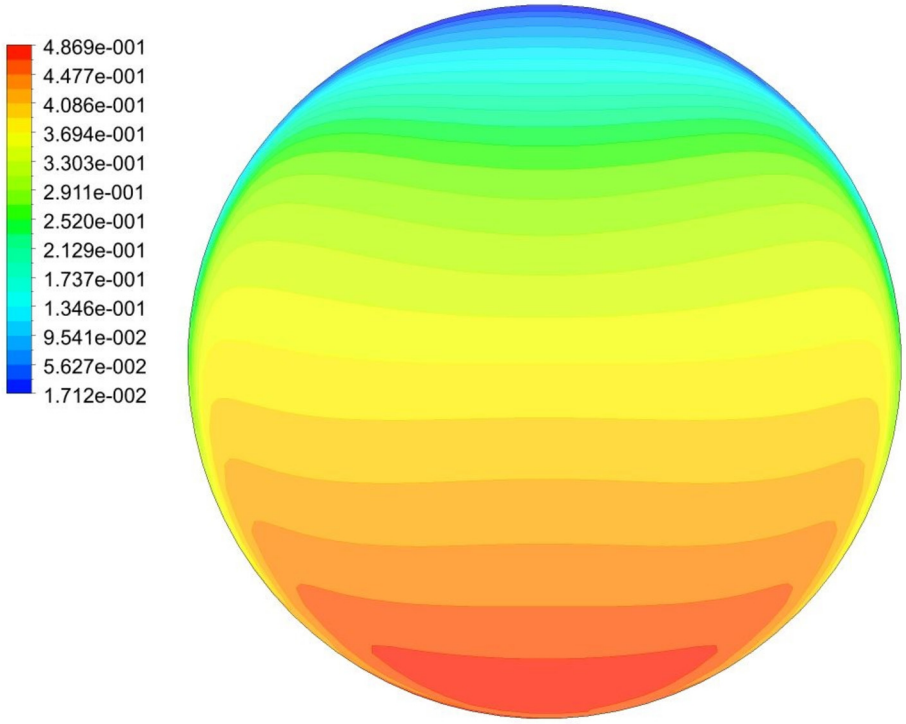

Fig. 14b. The concentration contour (C_v = 0.35, dp = 370 μm, D = 150 mm, V = 5.99 m/s).

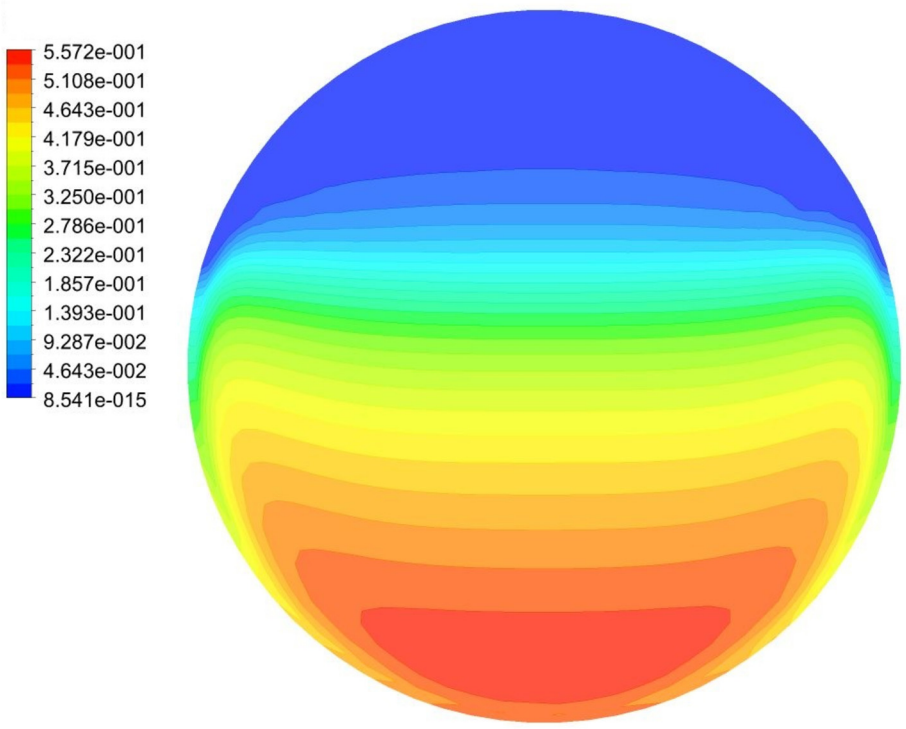

Fig. 15b. The concentration contour (C_v = 0.3, dp = 440 μm, D = 54.9 mm, V = 3 m/s).

Analytical solutions do not take this into account, but the CFD calculations do. The very small diffusivity near the pipe wall as a result of less turbulence near the pipe wall, resulting in hardly any diffusion near the pipe wall. This theory is correct for the turbulence diffusivity. However, if it is valid for the momentum diffusivity is questionable. Particles may behave independently of the eddies close to the pipe wall.

The assumption that the particle momentum diffusivity equals the turbulent diffusivity may be true for very small particles following the motions of the eddies, but if the particles become too large they may only follow the large eddies and not the small eddies. Very large particles will behave independently of the eddies. To make up for this flaw, The relation between the sediment momentum diffusivity ε_s and the turbulence diffusivity ε_m is established by using a diffusivity ratio β, according to Mukhtar (1991):

$$\varepsilon_s = \beta \cdot \varepsilon_m \tag{30}$$

Later, Kaushal and Tomita (2013) suggested a modified diffusivity ratio as shown in Eq. (17), where the diffusivity increases with the particle size.

$$\beta_{Kaushal} = 1 + 93.77 \cdot \left(\frac{d_m}{D_p}\right)\left(\frac{d_j}{d_{mw}}\right) \cdot e^{1.055 \cdot \sigma_g \cdot \frac{C_{vs}}{C_{vb}}} \tag{31}$$

In Eq. (17), d_m is the mean particle diameter, D_p is the Pipe diameter, d_j is the particle diameter j^{th}fraction of the particle size distribution (PSD), d_{mw} is the weighed mean particle diameter, σ_g is the PSD grading coefficient, C_{vs} is the spatial volumetric concentration, C_{vb} is the spatial volumetric concentration of the bed.

However, it is clear that they still use the advection-diffusion equation. It is a question whether this equation is still valid for larger particles.

In addition, as can be seen from Figs. 10–12. The volume fraction of particles along the direction of gravity increases gradually, and the maximum particle concentration appears at the bottom of the pipe. But in Figs. 13–15, with the increase of particle diameter, the concentration curve is observed to be reversed, and the maximum particle concentration moves away from the bottom of the pipe. According to the studies of Kaushal & Tomita (2007), Ekambara et al. (2009) and Gopaliya & Kaushal (2015), the near wall lift may be the reason. One of the explanations is, when the particle size exceeds the thickness of the viscous sublayer, which is inversely proportional to the line speed, the near wall lift force becomes dominant, so that the particles will move upwards from the pipe bottom. If the particle is bigger, the phenomenon may disappear because the increased gravity force will hamper lift.

6. Conclusions

This study initiates a new and comprehensive comparison between empirical equations and CFD model. Two different types of mathematical models (CFD and DHLLDV) have been studied to analyze the same physics: how fully-suspended slurries flow in pipeline. The following conclusions are obtained through the comparisons between calculated results and experimental data.

1 Both CFD and DHLLDV are qualified to calculate fully-suspended flow, with their good matches with experimental data, in terms of hydraulic gradient and concentration distribution. When the velocity is below the critical one, however, particle settling escalates and Euler-Euler model cannot apply to the flow regime, resulting in divergent results. Hence, a comparison among the CFD prediction, DHLLDV and experimental measurement at low flow velocities could not be made.
2 The choices of models according to different flow regimes will have significant impact on the obtained CFD results. For fully-suspended flow, Euler-Euler model in CFD can offer accurate calculations of hydraulic gradient. When flow regime changes from fully-suspended flow to sliding bed flow or fix bed flow, Euler-Euler model in CFD is likely to have deviation in the calculation of hydraulic gradient.
3 In the CFD calculation, the boundary conditions on the wall are very important for the concentration distribution near the wall and also for the calculation of pressure gradient. There will be a lot of efforts made to carefully tune the boundary condition on the pipe wall, since the CFD model focuses on the micro details inside the flow structure. As for the fine particles, both CFD and DHLLDV offer good

calculations of concentration distribution, but they have slight deviation for the near-wall area. As for large-sized particles, such deviation becomes more obvious in both CFD and DHLLDV, mainly because particles in near-wall area move differently in turbulent core area. The further research should improve the accuracy in simulating the particle movements in near-wall area.

To sum up, Euler-Euler model can give a good simulation to fully-suspended flow, with its good match to experimental data and careful micro-observation in flow, despite its inaccuracy for larger particles. DHLLDV is a generally recognized model and is better suitable for dredging engineering with its accuracy in calculated results, wide applicability to five typical flow regimes, less time consumption and higher speed in calculation despite its negligence in some flow details.

Acknowledgments

The authors are grateful for financial support from the Natural Science Foundation of China (No. 51709210).

References

Doron, P., Barnea, D., 1993. A three-layer model for solid-liquid flow in horizontal pipes. Int. J. Multiph. Flow 19 (6), 1029–1043.
Durand, R., Condolios, E., 1952. Experimental study of the discharge pipes materieaux especially products of dredging and slurries. Deuxiemes Journees de l'Hydraulique 27–55.
Ekambara, K., Sanders, R.S., Nandakumar, K., et al., 2009. Hydrodynamic simulation of horizontal slurry pipeline flow using ANSYS-CFX. Ind. Eng. Chem. Res. 48 (17), 8159–8171.
Gillies, R.G., Shook, C.A., 2000. Modeling high concentration settling slurry flows. Can. J. Chem. Eng. 78, 709–716.
Gillies, R.G., Shook, C.A., Xu, J., 2010. Modelling heterogeneous slurry flows at high velocities. Can. J. Chem. Eng. 82 (5), 1060–1065.
Gopaliya, M.K., Kaushal, D.R., 2015. Analysis of effect of grain size on various parameters of slurry flow through pipeline using CFD. Part. Sci. Technol. 33 (4) 1389346471.
Hayase, T., Humphrey, J.A.C., Greif, R., 1992. A consistently formulated QUICK scheme for fast and stable convergence using finite-volume iterative calculation procedures. J. Comput. Phys. 98 (1), 108–118.
Johnson, P.C., Jackson, R., 1987. Frictional-collisional constitutive relations for granular materials, with application to plane shearing. J. Fluid Mech. 176, 67–93.
Kaushal, D.R., Tomita, Y., 2007. Experimental investigation for near-wall lift of coarser particles in slurry pipeline using γ-ray densitometer. Powder Technol. 172 (3), 177–187.
Kaushal, D.R., Tomita, Y., 2013. Prediction of concentration distribution in pipeline flow of highly concentrated slurry. Part. Sci. Technol.: Int. J. 31 (1), 28–34.
Kaushal, D.R., Sato, K., Toyota, T., et al., 2005. Effect of particle size distribution on pressure drop and concentration profile in pipeline flow of highly concentrated slurry. Int. J. Multiph. Flow 31 (7), 809–823.
Kaushal, D.R., Thinglas, T., Tomita, Y., et al., 2012. CFD modeling for pipeline flow of fine particles at high concentration. Int. J. Multiph. Flow 43, 85–100.
Kumar, A., Gopaliya, M.K., Kaushal, D.R., 2016. Modeling of sand-water slurry flow through horizontal pipe using CFD. J. Hydrol. Hydromechanics 64 (2).
Matousek, V., 2002. Pressure drops and flow patterns in sand-mixture pipes. Exp. Therm. Fluid Sci. 26 (6–7), 693–702.
Messa, G.V., Malavasi, S., 2015. Improvements in the numerical prediction of fully-suspended slurry flow in horizontal pipes. Powder Technol. 270, 358–367 (Part A).
Miedema, S.A., 2016. The heterogeneous to homogeneous transition for slurry flow in pipes. Ocean Eng. 123, 422–431.
Miedema, S.A., 2017. Slurry Transport Fundamentals, A Historical Overview &The Delft Head Loss &Limit Deposit Velocity Framework.
Mukhtar, A., 1991. Investigations of the Flow of Multisized Heterogeneous Slurries in Straight Pipe and Pipe Bends. IIT, Delhi, India PhD Thesis.
Newitt, D.M., Richardson, M.C., Abbott, M., Turtle, R.B., 1955. Hydraulic conveying of solids in horizontal pipes. Trans. Inst. Chem. Eng. 33, 93–110.
Patankar, S.V., Spalding, D.B., 1972. A calculation procedure for heat, mass and momentum transfer in three-dimensional parabolic flows. Int.j.heat Mass Transfer. 15 (10), 1787–1806.
Richardson, J.F., Zaki, W.N., 1954. Sedimentation & fluidization: Part I. Transactions of the Institution of Chemical Engineering 32, 35–53.
Roco, M.C., Shook, C.A., 1983. Modeling of slurry flow: the effect of particle size. Can. J. Chem. Eng. 61 (4), 494–503.
Schaan, J., Sumner, R.J., Gillies, R.G., et al., 2000. The effect of particle shape on pipeline friction for Newtonian slurries of fine particles. Can. J. Chem. Eng. 78 (4), 717–725.
Wasp, E.J., 1963. Cross country coal pipeline hydraulics. Pipeline News 20–28.
Wilson, K.C., 1979. Deposition limit nomograms for particles of various densities in pipeline flow. Hydrotransport 6, 12 (Canterbury, UK: BHRA Fluid Engineering).

Nomenclature

A_{C_v}: Concentration factor
C_{vs}: Volumetric spatial concentration
C_{vb}: Spatial volumetric concentration bed
C_{vm}: Coefficient of virtual mass force
C_{td}: Coefficient of turbulent diffusive forces
C_l: Lift coefficient
D_p: Pipe diameter
d: Particle diameter
d_m: Mean particle diameter
d_j: Particle diameter jth fraction
d_{mw}: Weighed mean particle diameter
e_{ss}: Coefficient of restitution
F_d: Drag force
F_l: Lift force
F_k: Sum of the interfacial forces
F_{td}: Turbulent diffusive forces
F_{vm}: Virtual mass force
K_{sl}: Inter-phase drag coefficient
g: Gravitational constant
$g_{0,ss}$: Radial distribution function
p: Pressure shared by all phases
p_s: Solids pressure
R_{sd}: Relative submerged density
V_{ls}: Line speed
V_t: Terminal settling velocity of particles
$\overrightarrow{v_s}$: Velocity of solid phase
$\overrightarrow{v_l}$: Velocity of liquid phase
ρ_l: Density of liquid
ρ_s: Density of solid phase
ρ_m: Density of mixture
λ_l: Darcy-Weisbach friction factor
λ_m: Darcy-Weisbach friction factor mixtur
α_l: Concentration of liquid phase
α_s: Concentration of solid phase
$\overline{\overline{\tau}}_l$: Stress-strain tensor of liquid phase
$\overline{\overline{\tau}}_s$: Stress-strain tensor of solid phase
κ_c: Concentration eccentricity coefficient
β: Power of Richardson & Zaki equation
δ_v: Thickness viscous sub-layer
σ_{sl}: Turbulent Schmidt number
Θ_s: Granular temperature
ϕ_{ls}: Exchange of fluctuating energy
γ_{Θ_s}: Dissipation of fluctuating energy
k_{Θ_s}: Diffusion coefficient for granular energy
$\overline{\overline{\tau}}_s$: Stress-strain tensor of solid phase
ε_s: Sediment diffusivity
ε_m: Eddy momentum diffusivity
μ: Shear viscosity
G_k: Turbulent kinetic energy
σ_g: PSD grading coefficient
ΔL: Length of the pipeline
ΔP_m: Head loss of mixture
ΔP_l: Head loss of liquid
$\Delta P_{s,pot}$: Pressure required to compensate for potential energy losses
$\Delta P_{s,kin}$: Power required to compensate for kinetic energy losses